Observation of ¹⁵N + α resonant structures in ¹⁹F using the thick target in inverse kinematics scattering method

M. La Cognata,[1,*] M. Fisichella,[1] A. Di Pietro,[1] P. Figuera,[1] V. Z. Goldberg,[2] S. Cherubini,[1,3] J. P. Fernández Garcia,[4]
M. Gulino,[1,5] L. Lamia,[1,3] D. Lattuada,[1,6] M. Lattuada,[1,3] R. G. Pizzone,[1] G. G. Rapisarda,[1]
S. Romano,[1,3] R. Spartá,[1] C. Spitaleri,[1,3] D. Torresi,[1] A. Tumino,[1,5] and M. Zadro[7]

[1]*Laboratori Nazionali del Sud–INFN, Via S. Sofia 62, 95123 Catania, Italy*
[2]*Cyclotron Institute, Texas A&M University, College Station, Texas 77843, USA*
[3]*Dipartimento di Fisica e Astronomia Universitá di Catania, Via S. Sofia 64, 95123 Catania, Italy*
[4]*Departamento FAMN, Universidad de Sevilla, Apartado 1065, 41080 Sevilla, Spain*
[5]*Facoltá di Ingegneria e Architettura, Universitá di Enna Kore, Enna 94100, Italy*
[6]*Extreme Light Infrastructure-Nuclear Physics (ELI-NP), 30 Reactorului Street, 077125 Magurele, Romania*
[7]*Ruđer Bošković Institute, Bijenička cesta 54, 10000 Zagreb, Croatia*

The spectroscopy of ¹⁹F is of interest for nuclear astrophysics and nuclear structure. In astrophysics, fluorine and the reactions producing and destroying it play a key role in constraining models of stars in different evolutionary stages, such as the asymptotic giant branch (AGB) stars, responsible of the production of about half of the elements heavier than Fe. In nuclear structure, ¹⁹F has been subject to many investigations aiming at the identification of α and more exotic cluster structures. Also, its spectroscopy is very useful to constrain the nuclear properties of the ¹⁹Ne mirror nucleus. In this work, we report on the measurement of the ¹⁵N-α elastic scattering using the thick target inverse kinematics approach, allowing us to span a very large fluorine excitation energy range (∼6–10 MeV). The use of ¹⁵N-α scattering proves very useful to study α clustering in ¹⁹F thanks to the likelihood for populating states with such a structure. Indeed, the *R*-matrix analysis of the measured differential cross sections shows the occurrence of many candidate α-cluster states of ¹⁹F. It also calls for the redefinition of the spin-parity and widths of a number of ¹⁹F states with respect to what reported in the literature.

I. INTRODUCTION

¹⁹F has been the subject of many investigations, focusing on the study of cluster structures in $N > Z$ nuclei (see, for instance, Ref. [1] and references therein). In these systems, exotic cluster configurations may show up, having chemical-bonding-like structures. The ¹⁹F excitation energy spectrum has been analyzed using microscopic and semimicroscopic models as well as phenomenological potential models [2,3]. Essentially, ¹⁹F can be described as a one-proton-deficient system of ²⁰Ne, and thus the level sequence has been interpreted by considering the α-hole cluster model as well as the coupling of the $α + ^{15}$N and the $t + ^{16}$O channels [4,5]. Calculations performed using the generator-coordinate formalism [3] have shown that a good agreement is found with the ¹⁹F level sequence even without introducing the $t + ^{16}$O configuration, when assuming a coupling with the 3/2⁻ third excited state of ¹⁵N. It is also worth mentioning the recent work [6], addressing the occurrence of α clustering in the ¹⁹Ne mirror nucleus. The experiment showed that the majority of the observed levels have large α reduced widths, corresponding to fractions of the Wigner limit larger than

10%, thus providing evidence for predicted $α + ^{15}$O structures. The study of $α + ^{15}$N scattering can help us to better constrain the spectroscopy of ¹⁹Ne, even if uncertainties in the translation of properties of ¹⁹F to its mirror nucleus ¹⁹Ne may introduce significant errors in the prediction of the mirror nucleus resonance strengths [7].

The nucleosynthesis of ¹⁹F has also been the subject of many studies over the past several years. Indeed, in astrophysics its abundance might be used as a probe of stellar nucleosynthesis, since production and destruction rates are very sensitive to the stellar interior physical conditions (see Ref. [8] and references therein for an updated discussion on fluorine astrophysical relevance). In detail, asymptotic giant branch (AGB) stars are presently credited with providing the fluorine galactic supply, as demonstrated by direct observations in AGB stars [9] and in other environments, such as planetary nebulae [10] and carbon-enhanced metal-poor stars [11]. In AGB stars, fluorine synthesis takes place through the ^{14}N$(α, γ)^{18}$F$(β^+)^{18}$O$(p, α)^{15}$N$(α, γ)^{19}$F reaction chain [12] in the intershell region where the *s* process occurs as well. Therefore, constraining fluorine abundance would make it possible to cast light on the *s* process [13]. Recent direct and indirect studies have mainly focused on fluorine destruction in the outer, H-rich stellar layers through the ^{19}F$(p, α)^{16}$O

---

*lacognata@lns.infn.it

reaction [8,14–16] and in the intershell region through the $^{19}F(\alpha, p)^{22}Ne$ reaction [17,18], but more work is mandatory to reduce the uncertainty affecting fluorine production rate, approaching a factor of 2 at $T \lesssim 0.2$ GK [7]. In this context, the study of $^{15}N + \alpha$ elastic scattering is particularly important as the spectroscopic information deduced from the analysis of the corresponding cross sections can be used to constrain the resonance strengths and energies intervening in the calculation of the reaction rate.

The measurement of the $\alpha + ^{15}N$ scattering is a very useful tool to explore clustering in ^{19}F because of the tendency of this process for populating states with a $\alpha + ^{15}N$ character. From an experimental point of view, an exhaustive discussion about ^{19}F level sequence is given in Ref. [19]. The discussion reported therein and in more recent works, supplying new data (such as Ref. [7]) and presenting reanalysis of existing ones (in particular Ref. [20]), shows that ambiguities exist in the attribution of spin parities of some states and on the corresponding α partial widths. In addition, a quite limited energy range has been covered in those experiments. New experimental data are therefore necessary, spanning an extended energy interval and including both angular distributions along with excitation functions. With this respect, the thick target in inverse kinematics (TTIK) resonant scattering [21] is very well suited to scan a large energy range in the excitation function by using a single initial beam energy. In a gas-filled scattering chamber, as projectiles slow down in the gas, elastic scattering takes place across a broad range of center-of-mass (c.m.) energies and angles. While the impinging beam is in the gas, light-scattered particles reach the detectors due to their lower-rate of energy loss, allowing us to reconstruct the elastic-scattering excitation function.

II. MEASUREMENT THROUGH THE TTIK METHOD

The $^{15}N + \alpha$ elastic-scattering excitation function was measured by using the TTIK method [21]. The ^{15}N beam at 40.23 MeV, produced by the Tandem accelerator at the Laboratori Nazionali del Sud in Catania (Italy), was sent into the CT2000 2-m-diameter scattering chamber, filled with helium gas of nominal isotopic purity of 99.9999% at a pressure of 142 mbar in static conditions. The gas pressure and the temperature were measured, respectively, by two capacitance manometers, with an accuracy of 0.3%, and with a thermocouple device, with 1 K sensitivity. It was verified that the temperature did not change appreciably during the whole experiment and that the two manometers were always giving consistent pressure values within their accuracy. Moreover, in order to keep the gas as clean as possible, thus reducing possible air contamination due to microleaks, the chamber was completely emptied and refilled once every second day. The chamber was insulated from the beam line by means of a 4.3-μm-thick Havar foil window.

The detection apparatus (see Fig. 1) consisted of five ΔE-E silicon telescopes (T1–T5) used to measure the energy and identify the recoiling α particles, placed 800 ± 2 mm away from the chamber center. Each telescope was made of a 10-μm-thick silicon surface barrier detector (SBD), with an active area of 50 mm^2, as ΔE stage, and a 500-μm-thick SBD
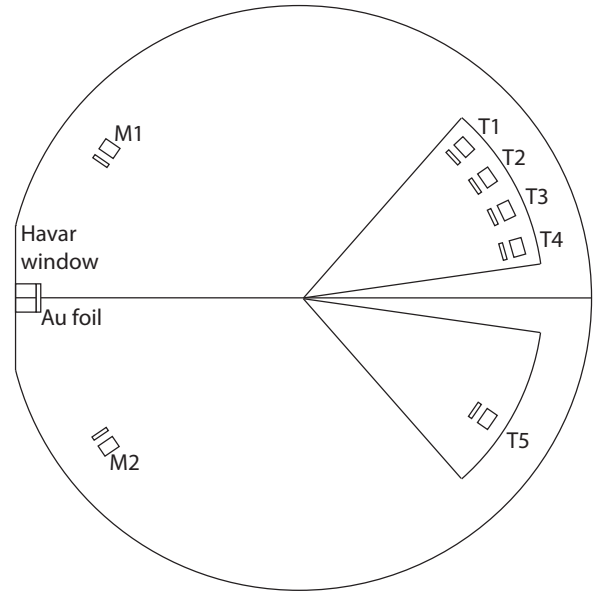

FIG. 1. Simplified sketch of the experimental setup. The scattering chamber is separated from the evacuated beamline by means of a 4.3-μm-thick Havar foil window. Right after it, a 200-μg/cm^2 gold foil was placed to measure elastically scattered ^{15}N particles in the monitor detectors M1 and M2. Five ΔE-E T1–T5 were mounted on two rotating plates.

to measure the residual energy. Four telescopes were mounted in the same rotating plate with an angular separation between two adjacent telescopes of about 5° with respect to the center of the chamber. The fifth telescope (T5) was placed in another rotating plate and was always symmetric with respect to T2, placed in the first plate. Two SBDs M1 and M2, 200 μm thick, were used to measure elastic scattering from a thin Au foil (200 μg/cm^2) placed downstream the Havar foil for normalization purposes. M1 and M2 were placed at $\pm 60°$ with respect to the gold foil (see Fig. 1). To avoid that the scattered beam on the windows could reach the monitors, a collimator between the window and the gold foil was placed. The trigger of the data acquisition was the logical or of all detectors.

The energy calibration of the E detectors was performed by using a three-peak (Am-Cu-Pu) α source and a ^{228}Th source, which emits α particles in an energy range from 5.34 to 8.68 MeV. Calibration runs with ^{14}N beam at 12 MeV on Au (203 μg/cm^2), C (62 μg/cm^2), and CD$_2$ (116 μg/cm^2) were also performed to calibrate ΔE detectors. These measurements were useful to check nominal values of the ΔE thickness, which is an important factor in the reconstruction of the α energy, as it will be discussed in the following. Monitor detectors were calibrated by using a three-peak α source.

The angular distributions were measured in steps of about 5° from 0° to 45° with respect to the center of the chamber. To cover this angular range, we used three different positions (configurations) of the plate. For each position, the angles (with respect to the center of the chamber) covered by each telescope are reported in Table I. In configurations 2 and 3 the telescope T4 covered the previous position of telescope T1; this, together with the T2–T5 symmetry, allowed us to

TABLE I. Measurement angles of each telescope with respect to the center of the scattering chamber. C1, C2, and C3 stand for configurations 1–3. All angles are expressed in degrees.

	C1	C2	C3
T1	15	30	45
T2	10	25	40
T3	5	20	35
T4	0	15	30
T5	−10	−25	−40

cross-check the experimental setup against systematic errors affecting solid angles, beam alignment, and arm movement. Consistent results were obtained, making it possible to rule out systematic uncertainties.

The excitation functions were reconstructed by considering as first interaction energy of ^{15}N the one after the gold foil ($E = 28.3$ MeV in the laboratory), removing the scattering events before it. Then elastic-scattering excitation functions were reconstructed as described below. The first step was the identification of α particles produced in elastic-scattering events. The use of ΔE-E detectors allows us to disentangle the presence of possible contaminants. However, in the present experiment only α particles were detected. Center-of-mass energy spectra were obtained from the energy deposited by the α particles in the residual energy detector and their angles with respect to the scattering position within the target. Energy loss of the beam and the recoiling α were calculated using the code SRIM [22]. Since only the residual energy of the α particle after the ΔE detector was used to deduce the excitation function, the calculation of their energy loss included, besides the E_{loss} in the gas, also the energy loss in the ΔE detector, detector dead layers, and gas in between the ΔE and E. For each detector telescope relations were found between the energy of the detected α particle and different quantities of interest: the position z of the interaction point along the beam direction, the center-of-mass energy $E_{c.m.}$, the angles θ_{lab} and $\theta_{c.m.}$, and the solid angle $\Delta\Omega_{lab}$ of the considered detector with respect to the interaction point in the target. For a given experimental α-particle energy, the values of these quantities, needed for the conversion of the measured spectra to the center-of-mass cross sections, have then been calculated by an interpolation procedure. Finally, the center-of-mass differential cross sections $d\sigma/d\Omega_{c.m.}$ were calculated. The number of incoming beam particles was obtained by using Rutherford scattering on the Au target, and the number of the scattering centers n_s was calculated from the target thickness $\delta z = z(E_a) - z(E_b)$ [where $z(E_a)$ and $z(E_b)$ are the interaction positions corresponding to the beginning and the end of the energy bin, E_a and E_b, respectively].

In Fig. 2, the center-of-mass excitation functions are given, for different configurations (C1–C3) and for each telescope (T1–T5), according to the scheme given in Table I, as a function of the ^{19}F excitation energy. It has to be underlined that in the excitation function the angle is a function of the center-of-mass energy. Indeed, when the detectors are not placed at zero degree, each center-of-mass energy corresponds

to a given distance z at which the scattering took place and then to a different scattering angle (see Fig. 3).

A. Evaluation of the energy resolution

The measured excitation function is affected by the energy and angular straggling of beam and scattered ions causing a smoothing of the measured cross section. The standard deviation σ of the Gaussian convolution function is a crucial aspect for spectroscopic applications as it influences the measured widths of the observed resonances. To evaluate such σ and its variation over the ^{19}F excitation energy range, the detection setup has been implemented into the GEANT4 and ROOT Object-Oriented Toolkit (GROOT) Monte Carlo tool [23]. GROOT relies on an external event generator (based on CERN ROOT libraries) while the tracking of particles is entirely based on GEANT4 and its classes. In this way, the straggling, both in angle and in energy, is simulated including all the interactions taking place while the impinging ^{15}N nucleus and the scattered α particle traverse the He-filled scattering chamber, until α's impinge on the telescopes. The results of the simulation is in agreement with the experimental energy resolution evaluated in Ref. [6], since at the energies of this experiment the energy losses calculated with SRIM [22] and GROOT essentially coincide. The variation of the energy resolution as a function of fluorine excitation energy is displayed in Fig. 4 for the telescope T4 set at zero degrees. In this figure, the energy spread expressed as the standard deviation of the Gaussian curve resulting from the straggling in the gas is given as a function of the center-of-mass energy and it does not include the detector intrinsic energy resolution (about 1%). At larger angles, the energy resolution quickly worsens as is evident from Fig. 2. The calculated energy resolution is accounted for in the performed R-matrix analysis. As such, in the following discussion a systematic uncertainty of the excitation energy and of resonance widths of about 15 keV (standard deviation) has to be considered.

To check the accuracy of the ^{19}F excitation energy reconstruction and of the evaluation of the energy resolution, we have smoothed the data from Ref. [24] at $\theta_{c.m.} = 169.1°$ (also used in the R-matrix analysis in Ref. [20]) to match the energy resolution evaluated using GROOT [23] and compared with the TTIK data corresponding to the C1T2 configuration [Fig. 2(b)], covering the $\theta_{c.m.} = 166° \pm 5°$ angular range, not much different from the angle in [24]. The results are shown in Fig. 5, where the data from the present work are given by solid circles and the smoothed data from Ref. [24] are shown as a solid red line. Extremely good agreement is clearly displayed by the comparison demonstrating the great accuracy of the analysis carried out in this work; the absence of any relevant model dependence since straggling and energy resolution, though connected, are evaluated with totally independent approaches. The estimated standard deviation between the two data sets corresponds to 15 keV, and this can be considered as a quantitative evaluation of the systematic error in the excitation energy, which is of the same order of the energy bin used in the analysis.

An additional test of the accuracy of TTIK method and of the results reported in the present work is given by the
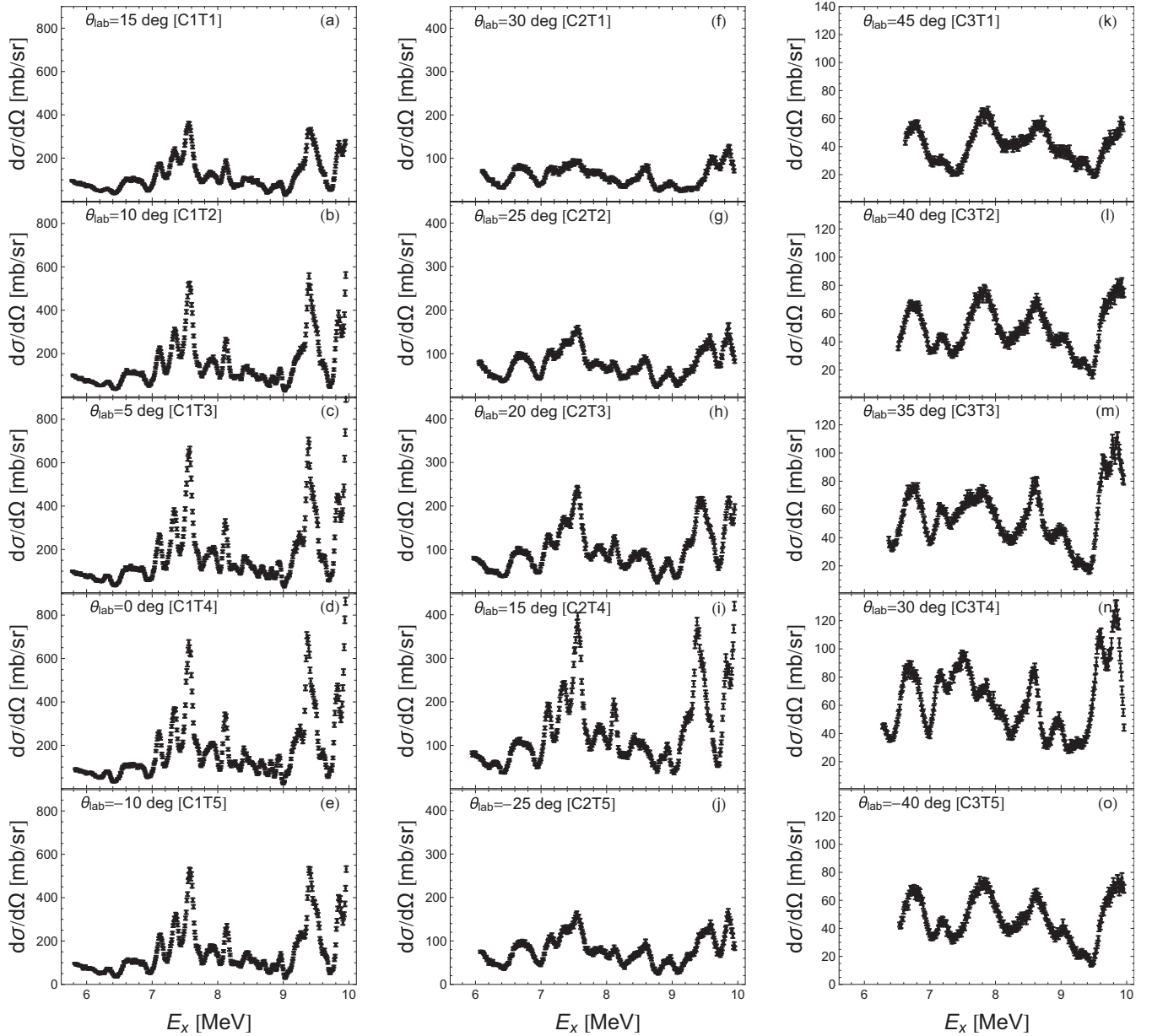
FIG. 2. Excitation functions of the ^{15}N $+ \alpha$ elastic scattering for different configurations (C1–C3) and for each telescope (T1–T5), as summarized in Table I. Cross sections are in the ^{15}N $+ \alpha$ center-of-mass system and expressed as a function of the ^{19}F excitation energy E_x. Statistical errors only are reported. The displayed angles ($\theta_{\rm lab}$) are measured with respect to the center of the scattering chamber.

comparison with the results in Ref. [25], where the excitation function of the ^{15}N $+ \alpha$ resonant elastic scattering is also displayed (see Fig. 6 of Ref. [25]). In Ref. [25], the TTIK technique was used with a different set-up, data-analysis procedure, and slightly better energy resolution with respect to the present one, yet the comparison of the measured cross sections at the same center-of-mass angle of $180°$ in Ref. [25] and in the present paper clearly shows a very good agreement.

III. *R*-MATRIX ANALYSIS

A *R*-matrix analysis of the ^{15}N$(\alpha, \alpha)^{15}$N excitation functions measured at $\theta_{\rm lab} = 0°$ (C1T4), $\theta_{\rm lab} = 5°$ (C1T3), $\theta_{\rm lab} = 10°$ (C1T2), and $\theta_{\rm lab} = 15°$ (C1T1), corresponding to the

data shown in Figs. 2(d), 2(c), 2(b), and 2(a), respectively, has been performed by means of the AZURE2 computer code [26,27]. We focus on the data at $\theta_{\rm lab} = 0°$–$15°$ (corresponding to α particles emitted at backward angles in the center of mass) since they show a significantly better energy resolution, making it possible to investigate in greater details the resonant structure of the ^{15}N$(\alpha, \alpha)^{15}$N cross section. The possibility to span the $\theta_{\rm c.m.} = 152°$–$180°$ angular interval makes it possible to identify the spin-parity of some resonances in the case of unknown or ambiguous attribution in the literature. Since the *p* channel opens at 7.9942 MeV, a two-channel multilevel analysis has been carried out, simultaneously fitting the mentioned ^{15}N$(\alpha, \alpha)^{15}$N excitation functions and the ^{18}O$(p, p)^{18}$O elastic-scattering data at $\theta_{\rm c.m.} = 140.8°$ [28].
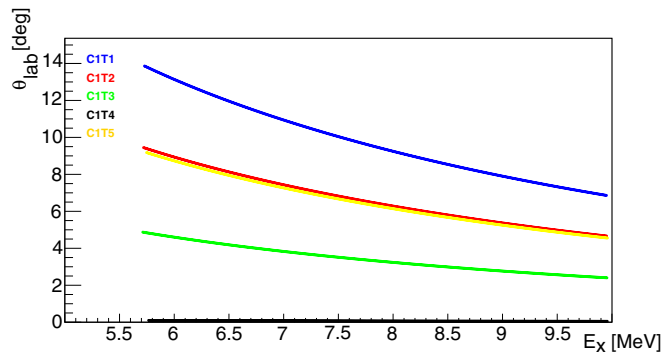
FIG. 3. Kinematic plot showing the connection between the ^{19}F excitation energy and the ^{15}N scattering angle in the laboratory for different detector configurations (Table I).

Since radiative capture is negligible at these excitation energies, the γ channel has been neglected in the analysis. In the fitting, the ^{15}N-α-channel radius R_α was taken equal to 5.27 fm, as calculated from the equation 1.3 $(A^{1/3}_{^4{\rm He}} + A^{1/3}_{^{15}{\rm N}})$, whereas the ^{18}O-$p$-channel radius R_p was taken equal to 4.71 fm, using an equivalent formula.

As a starting point, we have introduced in the calculation the ^{19}F states for which α decay has been observed, fixing the resonance energies and the resonance widths, in the case where these are known. Whenever upper or lower limits or even no values are given, we have left these widths as free fitting parameters (specifying in Tables II and III that the listed parameters come from data fitting). In the case when spin-parities are not known, we performed calculations with increasingly large values, in the attempt of reaching, at least, a qualitative agreement between the excitation functions and the fitted R-matrix function. In this preliminary calculation, a total of 70 resonances were used, falling in the $E_x = 5.7$- to 9.6-MeV excitation energy range. We focused on the C1T4
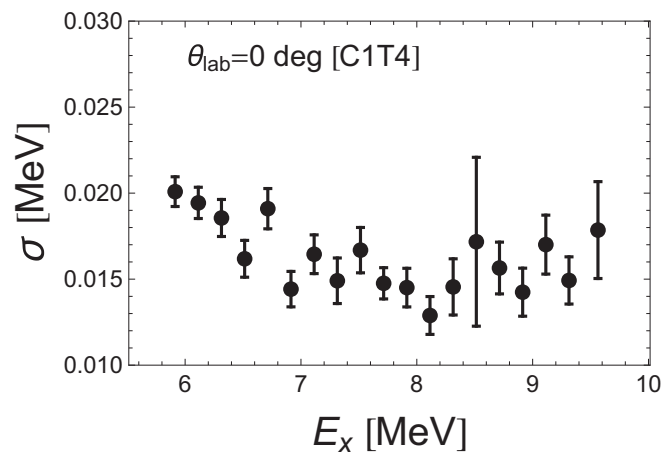

FIG. 5. Comparison between the ^{15}N-α elastic-scattering cross section as a function of ^{19}F excitation energy measured in this work (solid circles), corresponding to the C1T2 configuration [Fig. 2(b)] and the data from Ref. [24] at $\theta_{\rm c.m.} = 169.1°$ (solid red line), smoothed to match the energy resolution predicted by GROOT at the covered angular range.

data [Fig. 2(d)], due to their best resolution as calculated using the GROOT simulation code mentioned earlier. Twenty fitting parameters were present, leading to 392 degrees of freedom. The effect of resolution was taken into account by folding the R-matrix function with a Gaussian function [26,27]. The resulting R-matrix fitting curve is shown as a gray line in Fig. 6. A reduced $\tilde{\chi}^2 = 115$ for 392 degrees of freedom was obtained, demonstrating a very poor agreement between the calculation and the experimental data. This is apparent also by inspecting Fig. 6, urging us to analyze the causes of such patent incongruity. Therefore, we attempted to change the spin-parity of the states having uncertain spin and parity assignments or even none [19]. However, by no means it was possible to achieve a reasonable reproduction

FIG. 4. ^{19}F excitation energy spread expressed as the standard deviation of the Gaussian curve resulting from the straggling in the gas as a function of the ^{19}F excitation energy for the C1T4 configuration (see Table I and Fig. 2). The error bar (one standard deviation) reflects statistical uncertainty only. See text for details.
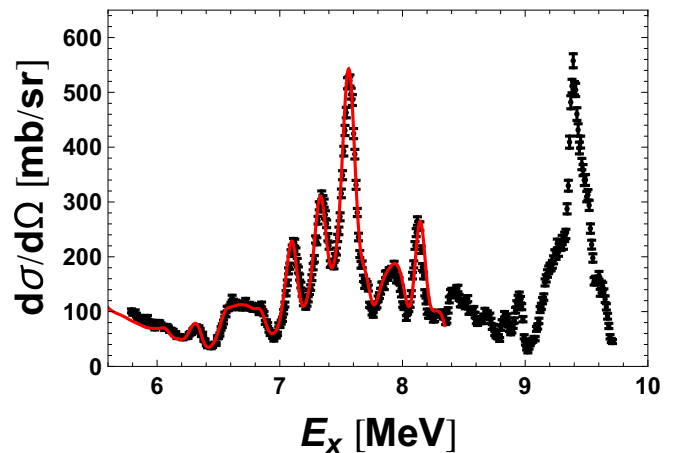

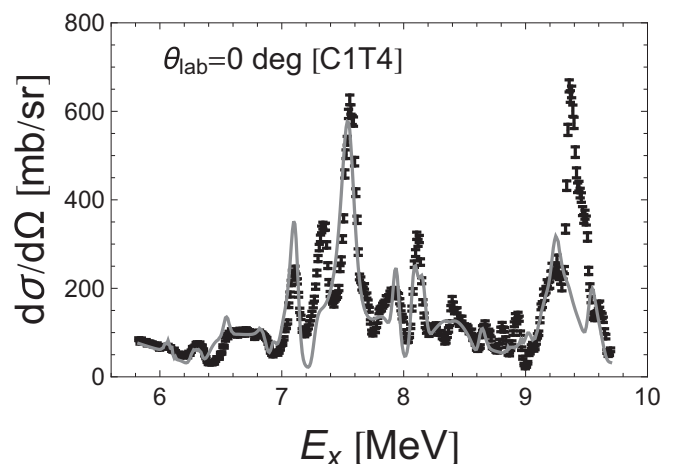FIG. 6. For the data in Fig. 2(d), a fit has been performed including the ^{19}F states as reported in Ref. [19] (gray line), as well as the spectroscopic information available therein.

TABLE II. List of the levels introduced in the calculations: Comparison between the literature [19] and the present work. Γ's are either fixed to the values in Ref. [19] or fitted to the experimental data. In parenthesis, the alternative spin-parity given in the literature and not used in the calculation of Fig. 6. Only levels below the ^{19}F $\rightarrow p + ^{18}$O threshold (7.9942 MeV) are shown.

	Ref. [19]			This work	
J^{π}	E_x (MeV)	Γ_{tot} (keV)	J^{π}	E_x (MeV)	Γ_{α} (keV)[a]
1/2+	5.938	1.4×10^{-8}[b]	1/2+	5.938	0.77
7/2+	6.070	1.2	7/2+	6.070	1.77
3/2−	6.088	4.0	3/2−	6.088	46.3
9/2−	6.100	2.7×10^{-1}[b]	9/2−	6.100	—[c]
7/2−	6.1606	3.7×10^{-3}	7/2−	6.1606	3.07
1/2+	6.255	8.0	1/2+	6.255	—[c]
5/2+	6.282	2.4	5/2+	6.282	4.62
7/2+	6.330	2.4	7/2+	6.330	6.66
1/2−	6.429	$2.8 \times 10^{+2}$	1/2−	6.429	559
3/2+	6.4967	1.8×10^{-1}[b]	3/2+	6.4967	0.726
11/2+	6.500	4.0×10^{-12}[b]	11/2+	6.500	0.202
3/2+	6.5275	4.0	3/2+	6.5275	13.9
7/2+	6.554	1.6	7/2+	6.554	—[c]
9/2+	6.592	7.6×10^{-3}	9/2+	6.592	2.84
3/2−	6.787	6.9×10^{-3}	3/2−	6.787	2.26
5/2+	6.8384	1.2	5/2+	6.8384	3.58
3/2−	6.891	$2.8 \times 10^{+1}$	3/2-	6.891	7.26
7/2−	6.9265	2.4	7/2−	6.9265	—[c]
1/2−	6.989	$5.1 \times 10^{+1}$	1/2−	6.989	84
7/2+	7.114	$3.2 \times 10^{+1}$	7/2+	7.114	18.6
11/2−	7.1662	6.9×10^{-3}	11/2−	7.1662	1.87
3/2+	7.262	$4.2 \times 10^{+1}$[b]	3/2+	7.262	—[c]
1/2+	7.364	1.6×10^{-9}[b]	5/2+	7.364	99.9
5/2+	7.5396	1.6×10^{-1}	5/2+	7.5396	12.0
7/2+	7.56	$1.2 \times 10^{+2}$[b]	7/2+	7.56	158
5/2−	7.587[d]	–	5/2−	7.587	—[c]
3/2+	7.6606	2.2×10^{-3}	3/2+	7.6606	—[c]
1/2−	7.702	1.4×10^{-1}[b]	1/2−	7.702	327
7/2− (5/2)	7.74	1.4×10^{-9}[b]	5/2−	7.74	73.7
7/2+ (9/2)	7.929	1.9×10^{-2}[b]	7/2+	7.929	263
11/2+	7.937	$1.3 \times 10^{+1}$[b]	11/2+	7.937	—[c]
5/2−	7.90[e]	$1.7 \times 10^{+2}$[b]	1/2+	7.979[b]	1.10

[a]All fitting parameters.
[b]From data fitting.
[c]Not appreciable with the present experiment resolution.
[d]Not included.
[e]No spin-parity attribution in the literature.

of the experimental data in the whole energy range and other solutions had to be assessed.

In particular, the following features are apparent.

(1) Reference [19] assigns $J^{\pi} = 1/2^{+}$ to the 7.364-MeV state of ^{19}F, yet a dip in the cross section arises, suggesting a wrong spin-parity selection.

(2) In the energy region between 8.5 and 9 MeV a remarkable divergence between the fit and the experimental data shows up. This is attributable to a number of reasons: In case levels are present, they might have a wrong energy collocation and/or spin-parity identi-

fication; otherwise, the introduction of a new peak is necessary to fit the spectra, at around 8.8 MeV. Indeed, Ref. [19] quotes a state at 8.7932 MeV that it is not supposed to α decay.

(3) Probably, the most striking feature of the measured cross section is the sharp peak laying at 9.36 MeV. The levels listed in Ref. [19] exhibit a gap 180-keV wide right at these energies, making it necessary to conjecture a resonance centered at 9.36 MeV to fit the data.

These flaws in the understanding of the ^{19}F excitation spectrum, regarding both known states and ^{19}F states not present in the literature, have triggered a new analysis of the ^{15}N(α, α)^{15}N excitation function.

Starting from these considerations, we have then run Azure to simultaneously fit the C1T1–C1T4 spectra and the ^{18}O(p, p)^{18}O elastic-scattering data at $\theta_{\text{c.m.}} = 140.8°$ [28], taking into account the effect of energy resolution. The results are shown in Fig. 7 and Fig. 8 for the ^{15}N + α and the ^{18}O + p elastic scattering, respectively, as red lines, while the fitting parameters are given in the right columns (labeled as "This work") in Table II [for states below the ^{19}F $\rightarrow p + ^{18}$O threshold (7.9942 MeV)] and in Table III for states above this threshold. Except in the critical region between 8.5 and 9 MeV [see point (2) of the discussion above], the overall agreement is fairly good, as it is apparent from the reduced $\tilde{\chi}^2 = 20$ of the C1T4 spectrum [Fig. 7(d)], which is significantly better than the previous results. Similar values for $\tilde{\chi}^2$ are found for the fitting of the other spectra: 14 for C1T3 [Fig. 7(c)], 12 for C1T2 [Fig. 7(b)], 10 for C1T1 [Fig. 7(a)], and 19 for the ^{18}O(p, p)^{18}O elastic-scattering spectrum.

Regarding the points highlighted above, we have modified the spin-parity assignment of the 7.364-MeV ^{19}F state. By setting $J^{\pi} = 5/2^{+}$ in the place of $1/2^{+}$, we get a very nice reproduction of the state with total width $\Gamma = 100$ keV (see Table II). The accuracy of such assignment is confirmed by the angular dependence of the cross section around $E_{\text{c.m.}} = 3.3$ MeV (corresponding to a ^{19}F excitation energy of about 7.3 MeV), in good agreement with the experimental data, covering 0–15° in the laboratory and 159–180° in the center-of-mass frame [see Figs. 7(a)–7(d)], a region very sensitive to the contributing angular momenta.

At higher excitation energies, around $E_x = 9.4$ MeV, a good fitting of the experimental data [see Figs. 7(a)–7(d)] is achieved introducing in the analysis a novel state at 9.374 MeV, $J^{\pi} = 13/2^{+}$, $\Gamma_{\alpha} = 20$ keV, and negligible p width ($\Gamma_p = 7 \times 10^{-8}$ keV), as reported in Table III. Also, the spin-parity of the adjacent level at 9.509 MeV had to be fixed to reach good agreement with the experimental spectra. Of the two values for spin and parity suggested in the literature [19], $J^{\pi} = 5/2^{+}$ and $7/2^{+}$, we considered $J^{\pi} = 5/2^{+}$ since it led to a better fit. Also in this case the possibility to span the 165°–180° center-of-mass angular range helped to single out the most likely J^{π} assignment. At larger angles in the laboratory frame [see Figs. 2(f)–2(o)], energy resolution progressively washes out the contribution of the individual levels and were not used in the data fitting at this stage.

TABLE III. List of the levels introduced in the calculations: comparison between the literature [19] and the present work. Γ's are either fixed to the values in Ref. [19] or fitted to the experimental data. In parenthesis, the alternative spin-parity given in the literature and not used in the calculation of Fig. 6. Levels above the ^{19}F → $p + ^{18}$O threshold (7.9942 MeV) are shown.

	Ref. [19]			This work		
J^π	E_x (MeV)	Γ_{tot} (keV)	J^π	E_x (MeV)	Γ_α (keV)[a]	Γ_p (keV)[a]
5/2+	8.0140[d]	–	5/2+	8.0140	0	0
9/2−[e]	8.084	$1.1 \times 10^{+1}$[b]	9/2-	8.084	8.06	0
1/2+	8.1377	1.1×10^{-9}[b]	1/2+	8.1377	1008	–[c]
7/2+[e]	8.16	$1.2 \times 10^{+1}$[b]	11/2+	8.1384[b]	22.2	0
5/2+	8.1990	2.3×10^{-8}[b]	5/2+	8.199	35.9	–[c]
7/2− (5/2)	8.2543[d]	–	5/2−	8.2543	0	–[c]
13/2−	8.288	2.2×10^{-3}[b]	13/2−	8.288	2.14	0
5/2+	8.3100	4.7×10^{-2}	5/2+	8.3100	3.59	–[c]
5/2+ (7/2)	8.370	7.5	7/2+	8.3745[b]	10.9	0
5/2+	8.5835	$9.0 \times 10^{+2}$[b]	5/2+	8.5835	–[c]	–[c]
3/2−	8.5919	2.0	3/2−	8.5919	659	–[c]
7/2−	8.629	9.3[b]	7/2−	8.629	–[c]	0
1/2+	8.65	$3.0 \times 10^{+2}$	1/2+	8.4585[b]	87.8	12.9
1/2+	8.7932[d]	46	1/2+	8.7932	0	52.8
9/2− (<9/2)	8.864	1.0	7/2+	8.9439[b]	3.10	0
3/2−	8.9267	3.6	3/2−	8.9267	–[c]	–[c]
11/2−	8.953	1.0	9/2−	8.953	20.1	0
7/2+ (5/2)	9.030	4.2	5/2+	9.030	43.8	0
7/2−	9.0997	5.7×10^{-1}	7/2−	9.0997	3.31	0.195
9/2+ (7/2+)	9.101	1.0	7/2+	9.101	93.6	0
1/2+	9.167	6.2	1/2+	9.167	–[c]	–[c]
3/2+	9.204	$1.02 \times 10^{+1}$	3/2−	9.204	–[c]	0
11/2+ (9/2+)	9.267	2.0	11/2−	9.267	2.36	0
7/2+	9.280	$2.8 \times 10^{+2}$[b]	9/2+	9.280	–[c]	0
3/2+	9.318	3.4	3/2+	9.318	695	–[c]
1/2+	9.321	5.0	1/2+	9.321	363	922
5/2+ (<5/2)	9.329	6.0	5/2+	9.329	–[c]	0
–	–	–	13/2+	9.3738[b]	19.6	–[c]
7/2+ (5/2+)	9.509	3.9×10^{-2}[b]	5/2+	9.509	54.7	0
5/2+	9.527	$2.8 \times 10^{+1}$	5/2+	9.527	57	3.11
5/2+	9.5364	6.3	5/2+	9.5364	2.03	50.7
3/2−	9.566[d]	26	3/2−	9.566	0	103
3/2−	9.575	$6.7 \times 10^{+1}$	3/2−	9.575	283	1.29
7/2+	9.586	8.9	7/2+	9.586	524	0.282
3/2+ (5/2)	9.642	8.0	3/2+	9.642	110	0
3/2− (5/2)	9.654	6	3/2−	9.654	–[c]	0
3/2+	9.6675	3.6	3/2+	9.6675	1.20	173
9/2+ (11/2)	9.710	<1	9/2+	9.710	–[c]	0
5/2−	9.820	0.3	5/2−	9.820	10.7	25.6

[a]All fitting parameters.
[b]From data fitting.
[c]Not appreciable with the present experiment resolution.
[d]Not included.
[e]No spin-parity attribution in the literature.

The fitting of the $E_{c.m.} = 4.4$- to 5-MeV energy interval, corresponding to ^{19}F excitation energies in the range 8.4–9 MeV, is more complicated, still showing a not-so-satisfactory agreement as elsewhere. In detail, we have set as fitting parameters the energies of the states at 8.370, 8.65, and 8.864 MeV and varied the spin-parity of these states and of the state at 8.953 MeV in an attempt to reach the best fit or considered the alternative J^π values in Ref. [19]. From the inspection of Figs. 7 and 8 it turns out that the general trend is well reproduced, while some small features are not properly reproduced by the fitting. More work is therefore necessary on the ^{19}F spectroscopy in this energy interval, especially in view of the astrophysical applications.
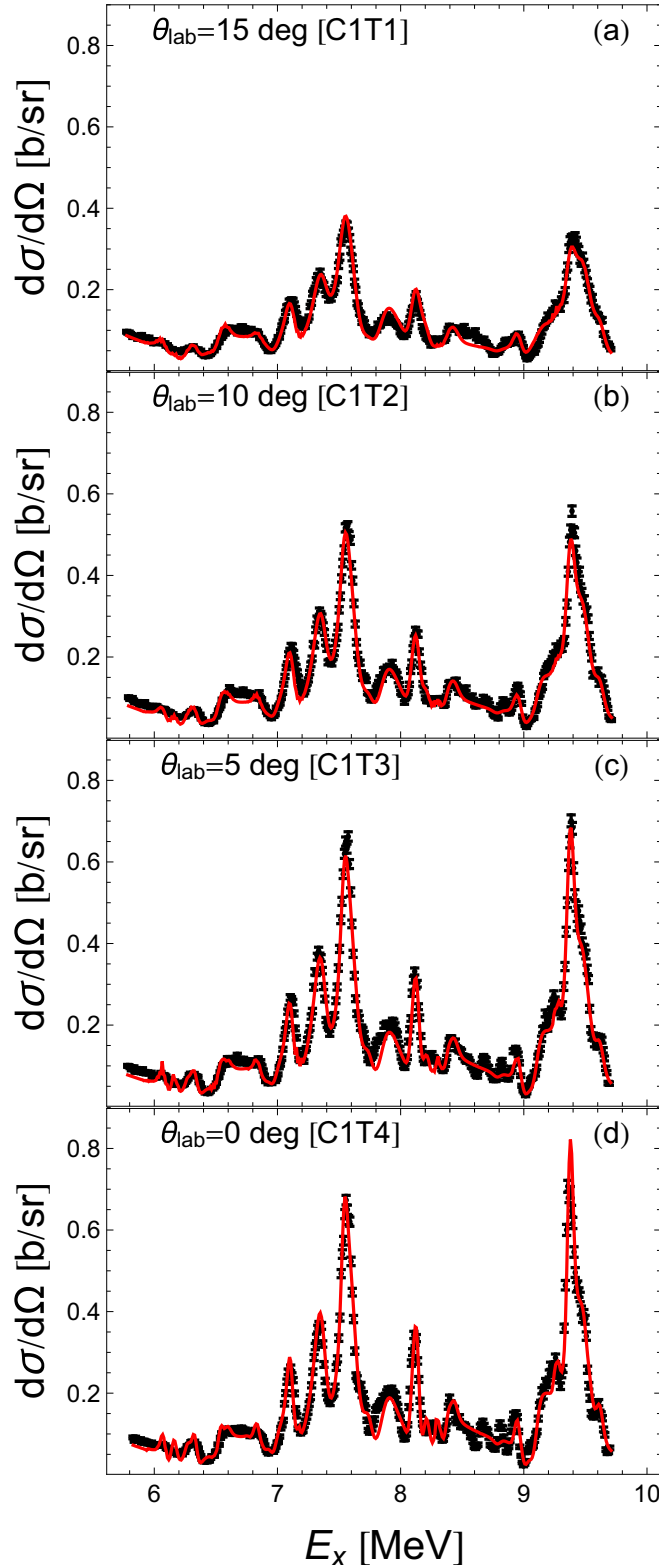
FIG. 7. *R*-matrix fit of the data in Figs. 2(d), 2(c) 2(b), and 2(a) (red line), superimposed on the experimental cross sections (black points).

Finally, it is worth noting that, in the fitting, additional poles at 30 MeV were considered, one per J^π entering the fit-
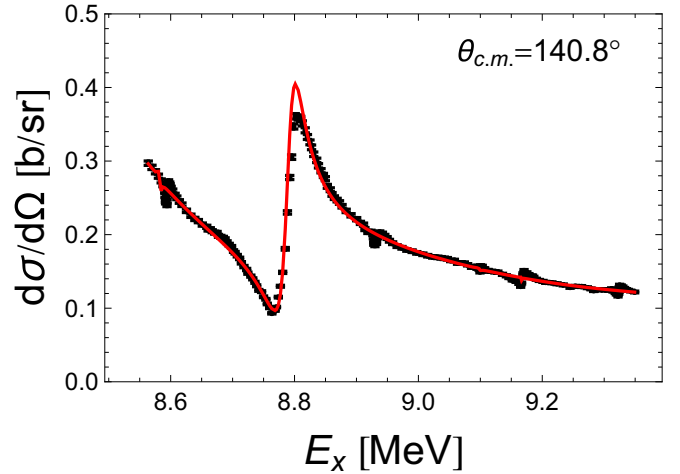

FIG. 8. *R*-matrix fit (red line) of the ^{18}O + p elastic-scattering data from Ref. [28] (black points). Data are reported against ^{19}F excitation energy.

ting, but their contribution is negligibly influencing the trend of the cross section and the values of the fitting parameters.

A. Comparison with potential model calculations

To investigate the α-cluster structure of the states contributing to the ^{15}N + α elastic-scattering excitation function, we have preliminarily adopted an approach similar to the one discussed in Ref. [6] to single out candidate cluster states. In detail, for each resonance in Tables II and III we calculated the ratio θ^2 of the α partial width Γ_α to the the corresponding Wigner single-particle limit [31] Γ_α^W. Following the prescription in Ref [6], values of $\theta^2 \gtrsim 0.1$ are assumed to indicate significant clustering; the states satisfying such condition are listed in Table IV and marked with green vertical lines in Fig. 9, where the ^{15}N + α elastic-scattering cross section at $\theta_{lab} = 0°$ (C1T4 configuration) is displayed. A very interesting feature is that the most prominent resonances in the excitation function all show a likely ^{15}N + α cluster structure configuration. In Table IV, θ^2 values $\gg 1$ signal a likely overestimation of the spin-parity for the corresponding states. These are the states at 6.592 and 7.166 MeV, having unrealistically large reduced widths $\gamma > 100$ MeV$^{1/2}$, calling for a reanalysis of the data in the literature. Regarding the 9.374-MeV state introduced in this work, for which a large $\theta^2 = 3.13$ value is obtained, a reduction of the spin-parity assignment to, for instance, $11/2^+$ causes an apparent worsening of the agreement with the corresponding experimental peak at all angles.

The reduced widths γ from the AZURE2 fitting are also compared with the single-particle reduced widths, calculated using the optical-model potential approach discussed in Refs. [29,30]. Since we are especially interested in the identification of α-cluster structure in ^{19}F, we introduced small changes in the computation; for instance, the channel radius was taken to be the same as in the *R*-matrix fitting. In all cases, the depth of the potential was adjusted to reproduce the resonance energy and the Coulomb potential was taken equal

TABLE IV. List of the levels from Tables II and III having $\theta^2 \gtrsim 0.1$. The fitting reduced width γ_{fit} and the corresponding values calculated using the potential model [29,30] are also given.

	J^π	E_x (MeV)	θ^2	γ_{fit} (MeV$^{1/2}$)	γ_{sp} (MeV$^{1/2}$)
1	7/2+	6.070	0.20	0.398	0.655
2	3/2-	6.088	1.01	$-$1.376	0.418
3	7/2-	6.1606	1.81	1.982	0.599
4	5/2+	6.282	0.24	0.440	0.532
5	7/2+	6.330	0.29	0.495	0.536
6	1/2−	6.429	1.12	2.153	1.019
7	9/2+	6.592	3.17	159.9	0.688
8	7/2+	7.114	0.11	0.293	0.757
9	11/2−	7.1662	3.65	368.4	0.308
10	5/2+	7.364	0.39	0.596	0.919
11	7/2+	7.56	0.45	0.659	0.940
12	1/2−	7.702	0.16	$-$0.345	1.033
13	7/2+	7.929	0.46	0.668	0.977
14	1/2+	8.1377	0.46	1.402	1.062
15	11/2+	8.1384	0.51	0.677	0.787
16	13/2−	8.288	0.27	0.462	0.321
17	3/2−	8.5919	0.33	0.518	0.919
18	11/2−	8.953	0.80	0.884	0.329
19	3/2+	9.318	0.20	0.382	0.804
20	1/2+	9.321	0.10	0.519	0.896
21	13/2+	9.3738	3.13	3.920	1.851
22	7/2+	9.586	0.26	0.653	1.045

to that of a uniformly charged sphere of radius R_α. For normalization and to assess of the validity of the model, the calculation was first performed for the 7.164-MeV 3^- state of ^{20}Ne,
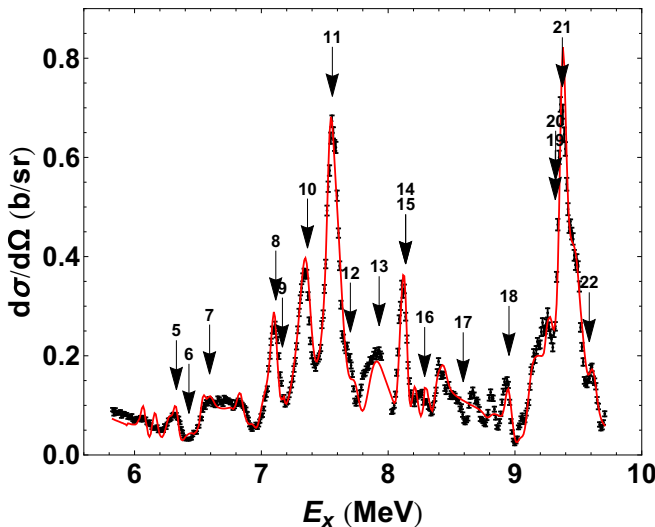

FIG. 9. R-matrix fit (red line) of the ^{15}N + α elastic-scattering data for the C1T4 detector configuration, corresponding to 0 degrees in the laboratory frame (black points). The vertical arrows highlight the ^{19}F states probably showing a ^{15}N + α cluster structure (numbers give the correspondence with Table IV). We only show the region above excitation energy $E_x > 6.3$ MeV where energy resolution is small enough to distinguish the contributing resonances.

showing a very strong α-cluster structure, $\theta^2 \approx 0.36$ and $\Gamma_{\alpha_0} = \Gamma_{\text{c.m.}} \approx 8$ keV [32]; a very good agreement with the experimental Γ_α was obtained assuming three nodes in the wave function. Similar results were obtained for other states in ^{20}Ne used to test this approach, in particular those at 10.262 MeV (5^-), 6.725 MeV (0^+), and 9.990 MeV (4^+).

In some cases, the single-particle reduced width depends on the number of nodes in the single-particle radial wave function; then, an average value was taken, even if the change was of the order of 10%, i.e., of the same magnitude of the experimental uncertainty. The resulting single-particle reduced widths γ_{sp}, calculated for the candidate cluster states, are given in Table IV. Calculations confirm the likely cluster-structure nature of the listed states while suggesting, for some states whose γ_{fit} exceeds the calculated one, a revision of the spin-parity assignment.

B. Comparison with previous analyses and ^{19}Ne mirror nucleus

The ^{15}N + α elastic scattering has been the subject of many investigations in the past years due to its importance, among others, in nuclear astrophysics. High-resolution data were reported in Ref. [24] that, however, stopped at energies lower than the p-emission threshold. The analysis of Ref. [20], mentioned in the Introduction, aimed at upgrading the R-matrix studies in Refs. [24,33] focusing, however, on a single backward center-of-mass angle of 169.1°. If we compare our results, summarized in Tables II and III, then we do not observe the shift in energy, about 7 keV, between the excitation energies extracted in the analysis of Ref. [20] and the accepted values in Ref. [19]. Conversely, we could obtain a nice fit of the experimental spectra in a wide range of center-of-mass angles by fixing, at least below the ^{19}F $\rightarrow$ ^{18}O + p threshold, the resonance energies to the ones listed in Ref. [19]. In detail, we found a larger width for the 6.429-MeV ^{19}F level than what was reported in Ref. [19], in disagreement with the result of Ref. [20]. We confirm the vanishingly small contribution of the 6.497-MeV state for which we also obtained $\Gamma_\alpha < 1$ keV, and of the 7.101-MeV state discussed in Ref. [20], which was not needed to fit the experimental spectra. For the 6.989-MeV ^{19}F state we confirm the energy recommended in Ref. [19], while the width, determined through our fit, is in better agreement with the value given in Ref. [20]. Finally, our analysis seems to suggest that the contribution of the 7.028 ± 0.004-MeV state, introduced in the analysis of Ref. [20] of the data in Ref. [24], is not necessary to fit the experimental spectra around the 7-MeV energy range (see Fig. 7). This might be due to the fact that the analysis in Ref. [20] takes into account a limited energy range, stopping close to 7-MeV excitation energy, as well as a single angle (while only qualitative agreement is found at other angles). Thus, it may happen that interference with other states lying at larger energies might not be taken into account in the analysis, and this effect can be particularly important given the predicted width of such state, about 100 keV. The present work, instead, allows us to span a broader angular and energy region, possibly making it possible to get more reliable results, especially in the case of broad resonances that are less affected by energy resolution effects. It is worth noting that, if the

fitting parameters given in Table I of Ref. [20] (superseding the compilation [19] in the examined energy region) are used as starting values for the fit in the present work, a significant improvement of the reduced $\tilde{\chi}^2$ by about 15% is attained, due to smaller deviations below about $E_x = 7$ MeV. This is a consequence of the of fact that the analysis of Ref. [20] was carried out on the 169.1° data of Ref. [24], which cover a small energy range up to $E_\alpha = 4$ MeV, corresponding to $E_x = 7.17$ MeV. However, in this energy region, the data of the present work do not show prominent resonances, if compared with the experimental spectra above $E_x = 7$ MeV, due to energy resolution effects, smoothing out the contribution of resonances smaller smaller the those lying above about $E_x = 7$ MeV. Therefore, the change in the starting values and the choice of the resonances used in the best-fit process do not influence the main conclusions of this analysis.

References [34–36] used the ^{2}H(^{18}F, ^{19}F)n n-transfer and the following ^{19}F α decay (only for Refs. [34,35]) to populate ^{19}F states, perform spectroscopic studies, and, especially, deduce spectroscopic factors. ODue to the use of a radioactive ^{18}F beam, energy resolution is not enough to deduce the observed states partial widths. In some cases, resolution is even not sufficient to separate neighboring states, as in the case of the states at 7.262 and 7.364 MeV. This might justify the disagreement between the spin-parity attribution for the 7.364-MeV state.

Recently, the work in Ref. [6] has explored an almost overlapping excitation energy range in the ^{19}Ne mirror nucleus, updating and extending the results of Ref. [37]; assuming isospin symmetry a comparison with these parameters is very useful. From the comparison of the results in Tables II and III with those in Table I of Ref. [37], a general agreement is found, if one considers the uncertainties affecting both the analysis in the present work (mainly related with the energy resolution) and those of Ref. [37], as well as the assumption of isospin symmetry. In detail, discrepancies are found for the 6.592- and 7.166-MeV states, which can be related to the small widths of these states, for which the TTIK approach may be not accurate enough. In the case of 7.364 MeV, the difference may arise from the different assignment of the spin-parity of this resonance. Regarding the 7.540-, 7.702-, and 7.929-MeV levels, our analysis attributes larger widths with respect to Ref. [37], while in the case of 7.661 MeV a smaller one is determined with the present R-matrix fit, still consistent with the upper limit in Table I of Ref. [37]. Extending the comparison to the resonances listed in Ref. [6] (see Table I), where the occurrence of previously unobserved ^{19}Ne states were suggested, especially above the ^{19}F proton emission threshold, the agreement is generally improved. The comparison is given in Table V.

From its inspection, while we find a good reproduction of most of the states observed for the first time in Ref. [6], we can see discrepancies at 7.153(7.262) MeV, 7.469(7.5396) MeV, 7.568(7.6606) MeV, and 8.223(8.199) MeV, where the first (second) number refers to ^{19}Ne (^{19}F) excitation energies. In the case of the 7.262- and 8.199-MeV states, we confirm the results of the works in the literature [19,37], for 7.5396 MeV we obtain a width that is intermediate between the results in Refs. [6,37], and for the 7.661-MeV level we found agreement

TABLE V. Comparison between the widths deduced in Ref. [6] for ^{19}Ne and the ones for ^{19}F extracted in the present work R-matrix analysis, assuming isospin symmetry.

^{19}Ne [6]			^{19}F this work		
J^π	E_x (MeV)	Γ_{tot} (keV)	J^π	E_x (MeV)	Γ_{tot} (keV)
3/2−	5.983	21(8)	3/2−	6.088	46.3
1/2− (1/2+)	6.197	16(7)	1/2+	6.255	–
5/2+	6.279	6(2)	5/2+	6.282	4.62
7/2+	7.030	12(3)	7/2+	7.114	18.6
3/2+	7.153	252(39)	3/2+	7.262	–
7/2+	7.378	121(9)	7/2+	7.56	158
5/2+	7.469	83(17)	5/2+	7.5396	12
(3/2+) (1/2+)	7.568	774(144)	3/2+	7.6606	–
9/2+	8.022	64(10)	7/2+	7.929	263
5/2+	8.223	377(34)	5/2+	8.199	35.9
13/2− (11/2+)	8.428	4(1)	13/2−	8.288	2.14
(9/2−) (7/2−)	8.680	3(1)	7/2+	8.9439	3.10
(11/2−)	8.790	4(1)	9/2−	8.953	20.1

with the width in Ref. [19], even if energy resolution does not allow us to draw a definite conclusion. In the case of the 8.022(7.929)-MeV and 8.790(8.953)-MeV states, the difference can be related to the different spin-parity assignment of the present work.

Finally, the TTIK approach has been applied to the ^{15}N-α scattering in the $E_x = 6.7$–7.7 MeV in Ref. [38]. Even the analysis is limited to a small energy interval, and a similar conclusion to the ones given in this work were drawn. In particular, there is good agreement between the two fitting of the 7.114-MeV state; also the two analyses show no evidence of $3/2^+$ ^{19}F levels in the 7.3- to 7.4-MeV range. Regarding the 7.353-MeV state, the inspection of the angular dependence of the measured excitation functions around 7.3 MeV (while the analysis of Ref. [20] was limited to a single angle) has suggested the occurrence of a state with a larger spin-parity of $5/2^+$, which may coincide with the 7.364-MeV state [19] or with the mentioned 7.353-MeV one, since energy resolution ($\sigma \approx 15$ keV) does not allow to discriminate the two states.

IV. CONCLUDING REMARKS

We have investigated the ^{15}N + α elastic scattering using the TTIK approach in a broad angular and energy range, exploring ^{19}F states above and below the p-emission threshold, which are of interest for astrophysics and nuclear structure. Energy resolution was evaluated by implementing the experimental setup in a GEANT4 Monte Carlo simulation, using a ROOT event generation routine. Using such values, we have fitted the spectra with the best energy resolution, which are those measured at small laboratory angles, using the AZURE2 R-matrix code. By using the resonance parameters in Ref. [19] as starting values in the fitting procedure and keeping the resonance energies fixed to the values in the literature (unless no reasonable fit was obtained), we were able to reproduce the experimental spectra in the $\theta_{c.m.} = 152°$–180° angular interval and in the ~6- to 10-MeV excitation energy range. By comparing the fitting reduced widths γ with the Wigner

single-particle limits and with the values obtained from a potential model calculation, we were able to identify a number of candidate α-cluster states as well as to identify possible wrong spin-parity assignments. Also, we could single out a ^{19}F level at 9.374 MeV, so far unobserved. Our results agree with the most prominent features examined in the analysis of Ref. [20]. More work is necessary to perform a better spin-parity assignment in the ambiguous cases and to extend the fit to larger angles in the laboratory system, corresponding to center-of-mass angles $\theta_{\text{c.m.}} < 150°$.

From the astrophysical point of view, the explored ^{15}N + α relative energies are still too large to affect fluorine nucleosynthesis in AGB stars, though the technique may supply interesting information in future experiments more focused at lower energies, making this work an effective proof of principle. On the other hand, we explore the ^{19}F excitation energy range close to the ^{18}O + p emission threshold. As such, the spectroscopy of ^{19}F here discussed can help us to constrain the ^{18}O(p, α)^{15}N reaction cited in the Introduction, of interest in the study of nucleosynthesis in massive stars (through the CNO cycle) and in other astrophysical environments (see Refs. [39,40] for more details). The consequences for astrophysics are presently under analysis.

[1] R. Otani, R. Kageyama, M. Iwasaki, M. Kudo, M. Tomita, and M. Ito, Phys. Rev. C **90**, 034316 (2014).

[2] S. Ohkubo and Y. Ishikawa, Phys. Rev. C **31**, 1560 (1985).

[3] P. Descouvemont and D. Baye, Nucl. Phys. A **463**, 629 (1987).

[4] F. Nemoto and H. Bandō, Prog. Theor. Phys. **47**, 1210 (1972).

[5] T. Sakuda and F. Nemoto, Prog. Theor. Phys. **62**, 1274 (1979).

[6] D. Torresi, C. Wheldon, T. Kokalova, S. Bailey, A. Boiano, C. Boiano, M. Fisichella, M. Mazzocco, C. Parascandolo, D. Pierroutsakou, E. Strano, M. Zadro, M. Cavallaro, S. Cherubini, N. Curtis, A. Di Pietro, J. P. Fernández Garcia, P. Figuera, T. Glodariu, J. Grebosz, M. La Cognata, M. La Commara, M. Lattuada, D. Mengoni, R. G. Pizzone, C. Signorini, C. Stefanini, L. Stroe, and C. Spitaleri, Phys. Rev. C **96**, 044317 (2017).

[7] S. Wilmes, V. Wilmes, G. Staudt, P. Mohr, and J. W. Hammer, Phys. Rev. C **66**, 065802 (2002).

[8] I. Indelicato, M. La Cognata, C. Spitaleri, V. Burjan, S. Cherubini, M. Gulino, S. Hayakawa, Z. Hons, V. Kroha, L. Lamia, M. Mazzocco, J. Mrazek, R. G. Pizzone, S. Romano, E. Strano, D. Torresi, and A. Tumino, Astrophys. J. **845**, 19 (2017).

[9] C. Abia, K. Cunha, S. Cristallo, and P. de Laverny, Astron. Astrophys. **581**, A88 (2015).

[10] M. Otsuka, H. Izumiura, A. Tajitsu, and S. Hyung, Astrophys. J. Lett. **682**, L105 (2008).

[11] S. Lucatello, T. Masseron, J. A. Johnson, M. Pignatari, and F. Herwig, Astrophys. J. **729**, 40 (2011).

[12] A. Jorissen, V. V. Smith, and D. L. Lambert, Astron. Astrophys. **261**, 164 (1992).

[13] M. Lugaro, C. Ugalde, A. I. Karakas, J. Görres, M. Wiescher, J. C. Lattanzio, and R. C. Cannon, Astrophys. J. **615**, 934 (2004).

[14] I. Lombardo, D. Dell'Aquila, A. Di Leva, I. Indelicato, M. La Cognata, M. La Commara, A. Ordine, V. Rigato, M. Romoli, E. Rosato, G. Spadaccini, C. Spitaleri, A. Tumino, and M. Vigilante, Phys. Lett. B **748**, 178 (2015).

[15] M. La Cognata, S. Palmerini, C. Spitaleri, I. Indelicato, A. M. Mukhamedzhanov, I. Lombardo, and O. Trippella, Astrophys. J. **805**, 128 (2015).

[16] M. La Cognata, A. M. Mukhamedzhanov, C. Spitaleri, I. Indelicato, M. Aliotta, V. Burjan, S. Cherubini, A. Coc, M. Gulino, Z. Hons, G. G. Kiss, V. Kroha, L. Lamia, J. Mrázek, S. Palmerini, Š. Piskoř, R. G. Pizzone, S. M. R. Puglia, G. G.

Rapisarda, S. Romano, M. L. Sergi, and A. Tumino, Astrophys. J. Lett. **739**, L54 (2011).

[17] R. G. Pizzone, G. D'Agata, M. La Cognata, I. Indelicato, C. Spitaleri, S. Blagus, S. Cherubini, P. Figuera, L. Grassi, G. L. Guardo, M. Gulino, S. Hayakawa, R. Kshetri, L. Lamia, M. Lattuada, T. Mijatović, M. Milin, D. Miljanić, L. Prepolec, G. G. Rapisarda, S. Romano, M. L. Sergi, N. Skukan, N. Soić, V. Tokić, A. Tumino, and M. Uroić, Astrophys. J. **836**, 57 (2017).

[18] G. D'Agata, R. G. Pizzone, M. La Cognata, I. Indelicato, C. Spitaleri, S. Palmerini, O. Trippella, D. Vescovi, S. Blagus, S. Cherubini, P. Figuera, L. Grassi, G. L. Guardo, M. Gulino, S. Hayakawa, R. Kshetri, L. Lamia, M. Lattuada, T. Mijatović, M. Milin, D. Miljanić, L. Prepolec, G. G. Rapisarda, S. Romano, M. L. Sergi, N. Skukan, N. Soić, V. Tokić, A. Tumino, and M. Uroić, Astrophys. J. **860**, 61 (2018).

[19] D. R. Tilley, H. R. Weller, C. M. Cheves, and R. M. Chasteler, Nucl. Phys. A **595**, 1 (1995).

[20] D. W. Bardayan, R. L. Kozub, and M. S. Smith, Phys. Rev. C **71**, 018801 (2005).

[21] K. P. Artemov, O. P. Belyanin, A. L. Vetoshkin, R. Wolskj, M. S. Golovkov, V. Z. Goldberg, M. Madeja, V. V. Pankratov, I. N. Serikov, V. A. Timofeev, V. N. Shadrin, and J. Szmider, Yad. Fiz. **52**, 634 (1990) [Sov. J. Nucl. Phys. **52**, 408 (1990)].

[22] J. F. Ziegler, " SRIM code" (2018) [http://www.srim.org].

[23] D. Lattuada, D. L. Balabanski, S. Chesnevskaya, M. Costa, V. Crucillà, G. L. Guardo, M. La Cognata, C. Matei, R. G. Pizzone, S. Romano, C. Spitaleri, A. Tumino, and Y. Xu, EPJ Web Conf. **165**, 01034 (2017).

[24] H. Smotrich, K. W. Jones, L. C. McDermott, and R. E. Benenson, Phys. Rev. **122**, 232 (1961).

[25] A. K. Nurmukhanbetova, V. Z. Goldberg, D. K. Nauruzbayev, G. V. Rogachev, M. S. Golovkov, N. A. Mynbayev, S. Artemov, A. Karakhodjaev, K. Kuterbekov, A. Rakhymzhanov, Z. Berdibek, I. Ivanov, A. Tikhonov, V. I. Zherebchevsky, S. Y. Torilov, and R. E. Tribble, Nucl. Instrum. Methods A **847**, 125 (2017).

[26] R. E. Azuma, E. Uberseder, E. C. Simpson, C. R. Brune, H. Costantini, R. J. de Boer, J. Görres, M. Heil, P. J. LeBlanc, C. Ugalde, and M. Wiescher, Phys. Rev. C **81**, 045805 (2010).

[27] https://azure.nd.edu/login.php.

[28] K. Yagi, K. Katori, H. Ohnuma, Y. Hashimoto, and Y. Nogami, J. Phys. Soc. Jpn. **17**, 595 (1962).

[29] C. Iliadis, Nucl. Phys. A **618**, 166 (1997).

[30] F. C. Barker, Nucl. Phys. A **637**, 576 (1998).

[31] T. Teichmann and E. P. Wigner, Phys. Rev. **87**, 123 (1952).

[32] D. R. Tilley, C. M. Cheves, J. H. Kelley, S. Raman, and H. R. Weller, Nucl. Phys. A **636**, 249 (1998).

[33] T. Mo and H. Weller, Nucl. Phys. A **198**, 153 (1972).

[34] N. de Séréville, A. Coc, C. Angulo, M. Assunção, D. Beaumel, E. Berthoumieux, B. Bouzid, S. Cherubini, M. Couder, P. Demaret, F. de Oliveira Santos, P. Figuera, S. Fortier, M. Gaelens, F. Hammache, J. Kiener, A. Lefebvre-Schuhl, D. Labar, P. Leleux, M. Loiselet, A. Ninane, S. Ouichaoui, G. Ryckewaert, N. Smirnova, and V. Tatischeff, Nucl. Phys. A **791**, 251 (2007).

[35] A. S. Adekola, C. R. Brune, D. W. Bardayan, J. C. Blackmon, K. Y. Chae, C. Domizioli, U. Greife, Z. Heinen, M. J. Hornish, K. L. Jones, R. L. Kozub, R. J. Livesay, Z. Ma, T. N. Massey, B. Moazen, C. D. Nesaraja, S. D. Pain, J. F. Shriner, Jr., N. D. Smith, M. S. Smith, J. S. Thomas, D. W. Visser, and A. V. Voinov, Phys. Rev. C **84**, 054611 (2011).

[36] R. L. Kozub, D. W. Bardayan, J. C. Batchelder, J. C. Blackmon, C. R. Brune, A. E. Champagne, J. A. Cizewski, U. Greife, C. J. Gross, C. C. Jewett, R. J. Livesay, Z. Ma, B. H. Moazen, C. D. Nesaraja, L. Sahin, J. P. Scott, D. Shapira, M. S. Smith, and J. S. Thomas, Phys. Rev. C **73**, 044307 (2006).

[37] C. D. Nesaraja, N. Shu, D. W. Bardayan, J. C. Blackmon, Y. S. Chen, R. L. Kozub, and M. S. Smith, Phys. Rev. C **75**, 055809 (2007).

[38] D. Kim, G. W. Kim, S. Y. Park, A. Kim, K. I. Hahn, K. Abe, O. Beliuskina, S. Hayakawa, N. Imai, N. Kitamura, Y. Sakaguchi, H. Yamaguchi, S. M. Cha, K. Y. Chae, M. S. Kwag, S. W. Hong, E. J. Lee, J. H. Lee, E. K. Lee, J. Y. Moon, S. H. Bae, S. H. Choi, S. Kubono, V. Panin, Y. Wakabayashi, N. Iwasa, D. Kahl, and A. A. Chen, J. Korean Phys. Soc. **73**, 265 (2018).

[39] M. La Cognata, C. Spitaleri, and A. M. Mukhamedzhanov, Astrophys. J. **723**, 1512 (2010).

[40] M. La Cognata, C. Spitaleri, A. Mukhamedzhanov, A. Banu, S. Cherubini, A. Coc, V. Crucilla, V. Goldberg, M. Gulino, B. Irgaziev, G. G. Kiss, L. Lamia, J. Mrazek, R. G. Pizzone, S. M. R. Puglia, G. G. Rapisarda, S. Romano, M. L. Sergi, G. Tabacaru, L. Trache, R. E. Tribble, W. Trzaska, and A. Tumino, Astrophys. J. **708**, 796 (2010).